All-optical atom trap as a target for MOTRIMS-like collision experiments

S. Sharma,[1] B. P. Acharya,[1] A. H. N. C. De Silva,[1] N. W. Parris,[1] B. J. Ramsey,[1] K. L. Romans,[1]
A. Dorn,[2] V. L. B. de Jesus,[3] and D. Fischer[1,*]

[1]*Physics Department and LAMOR, Missouri University of Science & Technology, Rolla, Missouri 65409, USA*
[2]*Max Planck Institute for Nuclear Physics, Saupfercheckweg 1, D-69117 Heidelberg, Germany*
[3]*Instituto Federal de Educação, Ciência e Tecnologia do Rio de Janeiro IFRJ/Campus Nilópolis, Rio de Janeiro, Brazil*

Momentum-resolved scattering experiments with laser-cooled atomic targets have been performed since almost two decades with magneto-optical trap recoil ion momentum spectroscopy (MOTRIMS) setups. Compared to experiments with gas-jet targets, MOTRIMS features significantly lower target temperatures allowing for an excellent recoil ion momentum resolution. However, the coincident and momentum-resolved detection of electrons was long rendered impossible due to incompatible magnetic field requirements. Here we report on an experimental approach which is based on an all-optical ^{6}Li atom trap that—in contrast to magneto-optical traps—does not require magnetic field gradients in the trapping region. Atom temperatures of about 2 mK and number densities up to 10^9 cm^{-3} make this trap ideally suited for momentum-resolved electron-ion coincidence experiments. The overall configuration of the trap is very similar to conventional magneto-optical traps. It mainly requires small modifications of laser beam geometries and polarization which makes it easily implementable in other existing MOTRIMS experiments.

I. INTRODUCTION

In the last three decades, cold target recoil ion momentum spectroscopy (COLTRIMS) [1,2] became an indispensable experimental tool in atomic physics revealing unprecedented insights into the correlated dynamics of atoms and their constituents as well as in their interactions with external fields. With this technique it is possible to measure momentum vectors of atomic fragments after ionization events with high resolution down to extremely small kinetic energies. Due to the detailed views into the motion of atomic particles, these spectrometers are also often dubbed "reaction microscopes" (ReMi). A key ingredient of reaction microscopes is the atomic or molecular target gas which has to be prepared at temperatures as low as possible. This is necessary since any statistical thermal motion in the initial state would impair the final momentum resolution of the ionized atoms. In most experiments, supersonic gas jets are employed forming a target beam with typical temperatures of a few Kelvin. In so-called magneto-optical trap recoil ion momentum spectroscopy (MOTRIMS) experiments, optical cooling is used in magneto-optical traps (MOTs) (for a review see [3]). Here, substantially lower temperatures (mK or below) can be achieved and target atoms can be prepared in excited and polarized states (e.g., [4–6]).

Magneto-optical traps require large magnetic-field gradients in the trap region. While the field affects the momentum measurements of recoil ions only slightly, it renders the momentum-resolved detection of electrons impossible. This apparent incompatibility of magneto-optical trapping and electron momentum spectroscopy has recently been resolved in a MOTReMi experiment [7]. Here, a quadrupole magnetic field is switched periodically on and off thereby alternating between magneto-optical trapping and data acquisition cycles. Despite the success of this approach the experimental challenges should not be underestimated. The switching of the magnetic field substantially complicates the design of the experiment, its operation, and the analysis of the data acquired with the setup. Eddy currents have to be considered, the data acquisition and fast field switching need to be synchronized, and temporal fluctuations induced by the field switching must be accounted for in the data analysis.

In this paper we report on an all-optical trap (AOT) which we implemented in the MOTReMi experiment. Similar to MOTs, the present cooling and trapping scheme relies on the interaction of atoms with near resonant light, but in contrast to MOTs no magnetic field gradient is required. Although the AOT has resemblances to earlier realized configurations [8–11], it stands out since the trap can be operated with homogeneous magnetic fields of more than 10 Gauss. This makes it an ideal target for collision experiments in reaction microscopes which could easily be implemented in other existing MOTRIMS experiments.

II. EXPERIMENT

This experiment was performed with the MOTReMi, which is a unique combination of a magneto-optical trap for target preparation and a fully equipped reaction microscope for the momentum-resolved detection of electrons and recoil ions. Here, only the components relevant for the trapping mechanism are briefly discussed. A more detailed description of the momentum spectrometer and its overall design can be found in Ref. [12].
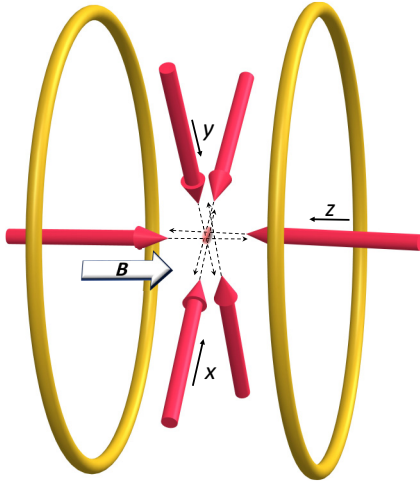
*fischerda@mst.edu

FIG. 1. Schematic view of the experimental setup. The retro-reflected laser beam pairs are slightly offset to one another. The magnetic field is collinear to the *z* axis and generated by a pair of Helmholtz coils outside the vacuum chamber.

The atom trap is located in a vacuum chamber with a background pressure of about 10^{-10} mbar and loaded with a cold beam of ^{6}Li atoms from a two-dimensional MOT. As in conventional magneto-optical traps, the atoms are cooled and trapped by three retro-reflected pairs of laser beams aligned along mutually (nearly) orthogonal axes. We chose the following coordinate system (see Fig. 1): Two laser beam pairs are oriented along the *x* and *y* directions, respectively. Due to the momentum spectrometer, the third pair is not precisely perpendicular to the *x* and *y* axis because particle detectors obstruct the optical access to the trap volume along the *z* axis (for details see [12]). Therefore, this beam has a small angle of 12.5° with respect to the *z* axis and points along the vector $(-\sqrt{2}\sin 12.5°, -\sqrt{2}\sin 12.5°, \cos 12.5°)$. For the MOT operation of the atom trap there is a pair of in-vacuum anti-Helmholtz coils which creates a quadrupole magnetic field in the trap region. However, for the trapping mode discussed here these coils were not in operation. Additionally, a homogeneous magnetic field in the *z* direction up to 15 Gauss can be generated with a large pair of Helmholtz coils (160-cm diameter) located outside of the vacuum chamber.

The laser beams are provided by a tapered-amplifier diode laser system whose frequency is stabilized slightly below the ^{6}Li *D2*-transition frequency from the $^2S_{1/2}$ ground state to the $^2P_{3/2}$ excited state ($\lambda = 671$ nm). The ground state of ^{6}Li has a hyperfine splitting of about 230 MHz. In order to avoid optical pumping to a dark state, the cooling beams need to contain two frequencies that excite transitions from both hyperfine levels. This is achieved by using an electro-optical phase modulator (EOM) producing sidebands shifted by ±230 MHz with respect to the cooler frequency (corresponding to the transition $^2S_{1/2} \rightarrow ^2P_{3/2}$ with the total atomic angular momenta $F = 3/2$ and $F = 5/2$, respectively). In the present experiment, the beams had diameters of about 10–15 mm with total powers of 15–25 mW. About 50% of the power is at the cooler frequency and 25% is up-shifted by 230 MHz to the re-pumper frequency ($^2S_{1/2}, F = 1/2 \rightarrow ^2P_{3/2}, F = 3/2$). Another 25% is shifted

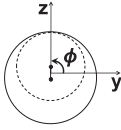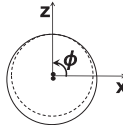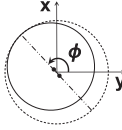230 MHz below the cooler frequency and not in resonance to either transition.

Compared to magneto-optical traps, the AOT is more sensitive to experimental parameters like beam positions, polarization, intensities, and frequency detuning. Similar to earlier reported configurations like the "supermolasses" [8] or the vortex trap [9], the positions of any two counterpropagating laser beams are slightly misaligned. Consequently, the adjustment of the beam positions and other parameters is not straightforward but is a tedious procedure. The general strategy to achieve stable trapping will be described in the following.

First, the atoms are trapped in a conventional MOT configuration. In this scheme, a quadrupole magnetic field is generated around the trap position with the anti-Helmholtz coils and all laser beams are circularly polarized by means of λ/4 wave plates with any two retro-reflected beams having opposite angular momentum ($\sigma^+ - \sigma^-$ configuration). Next, a homogeneous magnetic field in the *z* direction is superposed and stepwise increased up to about 7 Gauss. Due to this field the equilibrium position of the trap (i.e., of the local minimum of the magnetic field strength) shifts and the atom number drops. By adjusting positions, polarization, detuning of the beams, and the parameters of the atom source (i.e., the 2D MOT) the atoms' signal can (at least partially) be retrieved. Note that the trap position should stay unaltered compared to the initial MOT and should not shift with the zero magnetic field position. At sufficiently high magnetic fields the location of the atom cloud can only be retained if the polarization of the two laser beams along the *z* axis is identical because the Zeeman effect shifts the σ^+ transition to far from resonance which results in an imbalance of forces for the $\sigma^+ - \sigma^-$ configuration. Therefore, the λ/4 wave plate that flips the helicity of the retro-reflected *z* beam from σ^- to σ^+, has to be removed, which again makes a readjustment necessary. The configuration achieved in this way, resembles closely the spontaneous-force atom trap described by Walker *et al.* [10].

Thereafter, the quadrupole magnetic field is stepwise reduced and in each step all experimental parameters are again adjusted iteratively. When the quadrupole magnetic field is entirely switched off the λ/4 wave plates used for the beams in *x* and *y* directions can be removed and replaced by the λ/2 wave plate for each incoming beam. The trap was operated with two different laser polarization schemes. In the first one, referred to as the σ configuration, the beams parallel to the magnetic field were circularly σ^- polarized while the perpendicular beams were linearly polarized. For the latter the electric field vectors were perpendicular to the B field allowing only for the excitation of σ transitions. In the second scheme, in the following referred to as π configuration, all laser beams were linearly polarized with the polarization vectors of the transverse beams being parallel to the external magnetic field driving only π transitions.

Although stable trapping has been achieved for a large variety of experimental parameters, each configuration features a very narrow optimum, meaning a tiny variation of only one parameter can already result in the loss of the trapped atoms. All configurations had in common that the laser beams were misaligned relative to the trap center resulting in a vortex force. An example of laser beam parameters is listed in Table I.

TABLE I. Example set of laser beam parameters.

Coordinate axis	X	Y	Z'
Beam cross sections			
ingoing (solid)			
retro-reflected (dashed)			
Beam diameters (mm) (ingoing/retro-reflected)	11.5/8.5	10.6/9.6	11/13
Power (mW) (ingoing/retro-reflected)	24/21.6	16/14.4	18/16.2
Displacement (between beam centers)	1.5 mm	0.5 mm	1 mm
Angle ϕ of coaxal/ reference axis	$\sim 90°/Y$	$\sim 90°/X$	$\sim 135°/Y$

III. CHARACTERIZATION OF THE LASER-COOLED GAS CLOUD

The feasibility of highly differential atomic collision experiments depends strongly on target parameters such as the target density and temperature because these attributes influence the achievable coincidence rate and resolution, respectively. However, knowing the target cloud properties is not only important for the design and analysis of scattering experiments it also allows conclusions to be drawn on the trapping mechanism.

To characterize the ^{6}Li cloud we determined the trapped atom number, the number density, the characteristic loss and loading rates, the cloud temperature, and the polarization of the emitted fluorescence light. For most measurements fluorescence imaging was employed using three CMOS cameras positioned at relatively small angles (10° to 20°) with respect to the x, y, and z axes, respectively. For the measurement of the atom number we used additionally absorption imaging and obtained a consistent result. Some of the measured properties are listed in Table II. Measurements with the σ configuration are discussed in detail below.

A. Atom number and density

With the AOT, trapped atom numbers of about 10^7 are observed corresponding to number densities of 10^9 cm^{-3} in

TABLE II. Typical properties of the gas cloud.

	σ configuration	π configuration
No. of trapped atoms (N_{eq})	$\sim 10^7$	$\sim 10^7$
No. density	$\sim 10^9$/cm^3	$\sim 10^9$/cm^3
Temperature		
X axis	2.5 mK	2 mK
Y axis	700 μK	2 mK
Z axis	2 mK	>5 mK
Observed transitions		
σ^-	93%	43%
π	5%	43%
σ^+	2%	14%
Degree of polarization	90%	29%

a cloud of 1–2 mm in diameter. While such a target density is high enough for the study of interactions with high-intensity charged-particle or photon beams in collision experiments it is still substantially lower than the densities in other magneto-optical traps which are typically higher by a factor of 10–100. In order to identify the factors limiting the maximum atom number in the present configuration, the loss mechanisms and the loading rate of the ^{6}Li atoms were studied.

Generally, the trapped atom number N follows the simple rate equation,

$$\frac{dN}{dt} = L - \Gamma N - \beta \int n(\vec{r})^2 d^3 r, \quad (1)$$

with the loading rate L, the linear loss factor Γ (e.g., due to collisions with the residual gas), and the two-atom loss coefficient β due to mutual collisions between two excited lithium atoms. For not too high densities, the two-atom loss term can be approximated by $\beta' N^2$. This approximation is valid if the shape of the density distribution $n(\vec{r})$ does not change with the total atom number N (in MOTs this condition is typically fulfilled for densities below about 10^{10} cm^{-3} [13]). In this case, the loading rate L, the linear loss factor Γ, and the effective two-atom loss factor β' can easily be measured switching the atom beam from the 2D-MOT on and off thereby alternating the loading rate L between zero and its maximum value.

The general solution of the differential Eq. (1) can be expressed in the form,

$$N(t) = N_{eq} \frac{1 - \nu \xi e^{-\gamma t}}{1 + \xi e^{-\gamma t}}, \quad (2)$$

with the equilibrium number of atoms $N_{eq} = N(\infty)$ being

$$N_{eq} = \frac{\sqrt{4\beta' L + \Gamma^2} - \Gamma}{2\beta'}, \quad (3)$$

and with the coefficients $\gamma = 2\beta' N_{eq} + \Gamma$ and $\nu = L/(\beta' N_{eq}^2)$ as well as $\xi = (N_{eq} - N(0))/(\nu N_{eq} + N(0))$. For the following discussion, two situations are of special interest. First, the drop-off of the atom number initially being $N(0) = N_0$ after setting $L \to 0$.

$$N(t) = \frac{N_0 e^{-\Gamma t}}{1 + N_0 \beta'/\Gamma - N_0 \beta' e^{-\Gamma t}/\Gamma}. \quad (4)$$
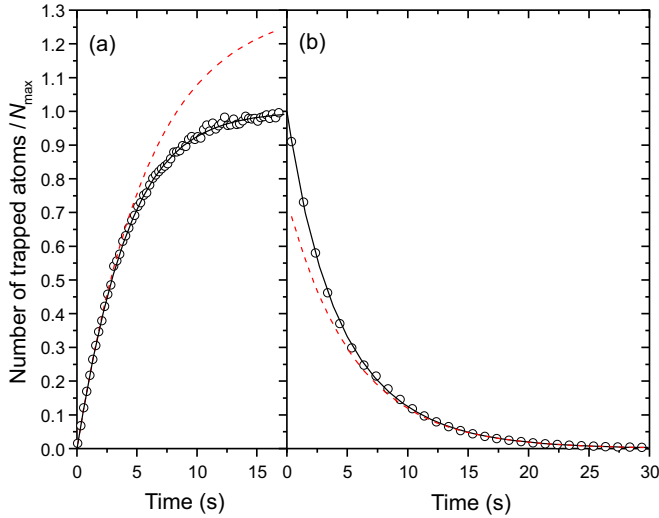
FIG. 2. Loading (a) and depletion (b) curve of the trap. Experimental data are shown as open circles; the solid lines correspond to the fits according to Eqs. (4) and (5), respectively. The dashed lines are exponential curves fitting the data for low atom number densities (i.e., where the two-atom loss term is negligible).

The second scenario is the loading of the initially empty trap, i.e., $N(0) = 0$ and $L > 0$, where the atom number follows the curve,

$$N(t) = N_{eq} \frac{1 - e^{-\gamma t}}{1 + e^{-\gamma t}/\nu}. \tag{5}$$

In Figs. 2(a) and 2(b), the atom trap population is shown as a function of time for the loading and the decay of the trap, respectively. The fits using Eqs. (4) and (5) show excellent agreement with the experimental data, while a pure exponential fit (i.e., assuming $\beta = 0$) describes the data only for very low atom numbers. Both the loading and the decay curve contain information on the Γ as well as the β' parameter and there is reasonable agreement between the two independent fitting results. For the data shown in the figure, the loading rate is about $L \sim 10^6/s$, the linear decay rate is about $\Gamma \approx 0.17/s$, and the effective two-atom loss rate is roughly $\beta' \sim 10^{-8}/s$, meaning that for a fully loaded trap about every fourth atom is lost due to mutual ^{6}Li collisions. Assuming a three-dimensional Gaussian distribution for the atom cloud density, the two-body loss coefficient can be calculated from β' and it is $\beta \sim 10^{-10}$ cm^3/s. Compared to earlier standard magneto-optical lithium traps (e.g., [14]), the present trap features Γ and β parameters which are only slightly higher indicating that the effective trap potential is shallower than those of conventional MOTs.

In order to compare AOT and standard MOT directly, a series of loading and depletion measurements were performed for both configurations. While the beam positions and the relative power distribution between the beams in x, y, and z directions were very different for AOT and MOT, the total maximum laser power was in both cases identical. The field intensity dependence of the Γ and β' parameters was tested by reducing the power of all laser beams proportionally (Fig. 3).

As it can be seen from the figure, Γ and β' are generally smaller for the MOT indicating that the effective trapping
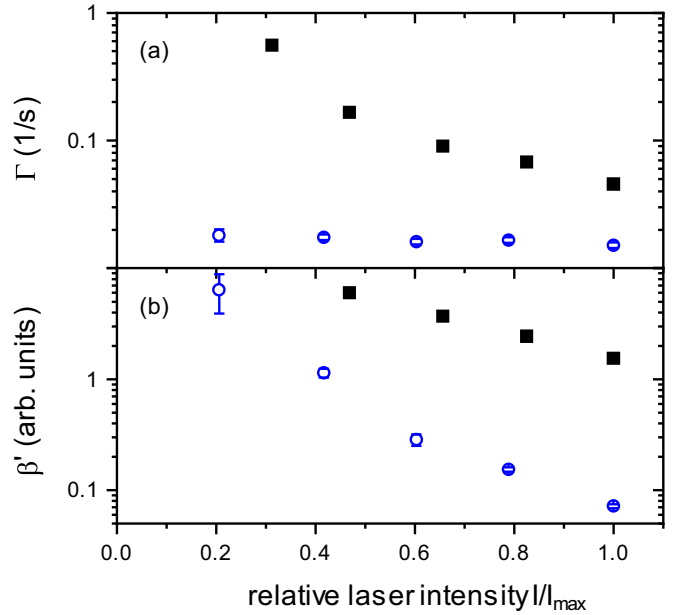

FIG. 3. Trap decay rate Γ (top) and effective two-atom loss coefficient β' (bottom) for AOT (full squares) and standard MOT (open circles) as a function of relative laser intensities (see text).

potential is shallower for the AOT. For the MOT, the measured trap decay rate Γ is saturated with the laser intensity and changes only marginally. In contrast, the two-atom loss rate β' increases significantly when the laser beam intensity is reduced. Such a behavior has been observed earlier and it was attributed to fine-structure changing collisions between excited lithium atoms [15]. For the AOT, both parameters Γ and β' depend strongly on the laser intensity and saturation is observed for neither of them in the investigated intensity regime. This indicates that higher trapped atom numbers can be expected by further increasing the overall laser intensity.

With the present setup the trapped atom number for the MOT configuration is typically about a factor of 5–10 higher than the AOT. However, in either configuration the atom numbers are substantially lower than reported for earlier lithium MOTs [14,16], because the loading rate L is about 2–3 orders of magnitude lower. This has to be attributed to the low atom flux of the loading beam. The design of the present atom source is very similar to the 2D-MOT described in Ref. [16], however, the available laser beam power for the trapping and pre-cooling of the atoms is a factor of 5 lower resulting in a substantially reduced cold atom flux. According to Eq. (3), enhancing the loading rate to $L = 10^9/s$ would lead to an increase of number density to almost 10^{11} cm^{-3} (neglecting the effect of geometrically increasing the trap size for high number densities [13]).

B. Cloud temperature

The temperature of the atoms was determined by measuring the ballistic expansion of the cloud when no forces are exerted on the atoms. To this end, the cooling lasers were switched off for short periods t and the width of the cloud was determined
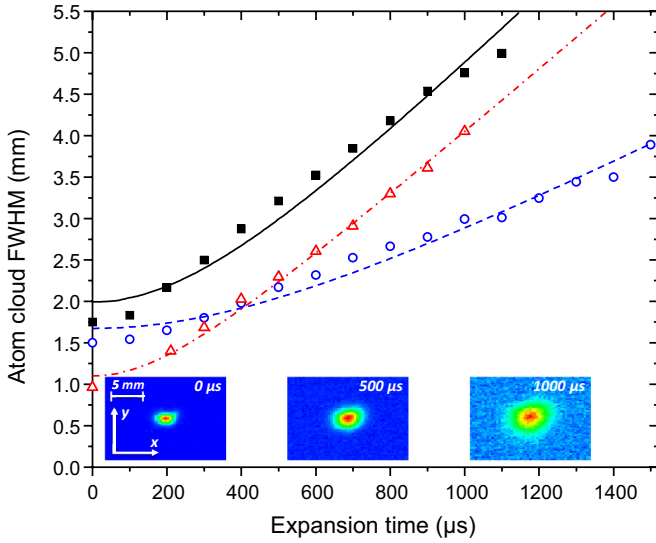
FIG. 4. Thermal expansion of the atom cloud. The cloud width is plotted as a function of the expansion time. The symbols represent the experimental data for the x (squares), y (open circles), and z directions (open triangles). The solid, dashed, and dash-dotted lines depict the respective fitting curves. Images from one of the CMOS cameras are shown as insets for expansion times of 0, 500, and 1000 μs.

FIG. 5. Zeeman splitting of the $^2S_{1/2}$ ($F = 3/2$) and the $^2P_{3/2}$ levels of ^{6}Li (from [17]).

after the switch-off by fluorescence imaging. In Fig. 4, the cloud widths in x, y, and z directions are plotted as a function of the time t. For a gas initially in thermal equilibrium (more precisely, the initial six-dimensional phase-space distribution of the gas being represented by a simple product of six Gaussians, one for each component) the spatial distribution along each axis for any given time t should be well reproduced by the convolution of two Gaussians, the first representing the initial distribution and the second the thermal expansion. The corresponding fitting curves are shown as lines in Fig. 4. From the fit, the thermal velocity and thus, the temperature of the gas can be extracted.

There are two notable observations made in the temperature measurements: First, the temperature is not identical along the three coordinate axes. The analysis yields about 2 mK in the x and z directions and about 700 μK in the y direction. These temperatures are substantially larger than the Doppler temperature (140 μK for ^{6}Li). Second, the fitting model used has a relatively poor agreement with the experimental data for the first 200–300 μs after switching the lasers off. Both observations can be explained by a vortex motion of the atoms due to the misalignment of the laser beams. This motion results in higher velocities in the plane of rotation leading to higher temperatures in the x-z plane. Moreover, the velocity distribution becomes dependent on the atoms' position resulting in a more complex time dependence than is expected with our fitting model.

C. Atomic polarization and laser frequencies

^{6}Li features a complex multilevel structure with two hyperfine levels in the $^2S_{1/2}$ ground state ($F = 1/2$ and $3/2$) and three hyperfine levels in the excited $^2P_{3/2}$ state ($F = 1/2$, $3/2$, and $5/2$). In contrast to heavier alkali-metal atoms such as rubidium
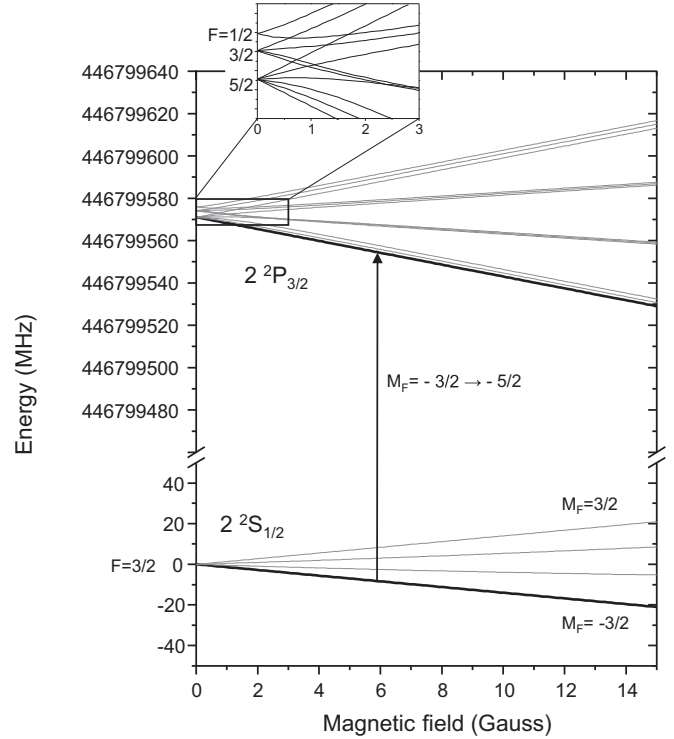
or cesium, the energy separation of the excited hyperfine levels in lithium is too small to be resolved by the cooling laser beams. This makes it generally more challenging to disentangle the distribution of populated states. Nevertheless, there are at least three ways to obtain information on the involved transitions and the atomic orientation: first, the polarization of the cooling laser beams; second, the influence of the laser frequencies on the trapping efficiency and the dependence on the strength of the external magnetic field; and third, the polarization of the emitted fluorescence light.

The energy of the involved magnetic sublevels for the three excited $^2P_{3/2}$ hyperfine states as well as for the $^2S_{1/2}$ hyperfine ground state ($F = 3/2$) are shown in Fig. 5 as a function of the magnetic field strength. For the excited P state and for magnetic fields of more than a few tenth of one Gauss the nuclear spin I and the electron angular momentum J decouple. For magnetic fields stronger than about 3 Gauss, the 16 levels are grouped in sets of three each corresponding to a specific M_J ranging from $-3/2$ to $+3/2$. The three states in each group represent the three possible orientations of the nuclear spin with M_I being -1, 0, or $+1$. It should be noted, that the z component of the total atomic angular momentum M_F is well defined for each eigenstate even though the absolute magnitude F is not necessarily a good quantum due to the mixing in the magnetic field. Hence, each line in the graph corresponds to a specific M_F irrespective of the magnetic field strength.

In the present σ configuration, the laser beams oriented along the z direction (which is the quantization direction) are circularly polarized driving only σ^- transitions (i.e., $\Delta M_F = -1$). The other laser beams are linearly polarized with their electric field vectors being perpendicular to the z axis allowing
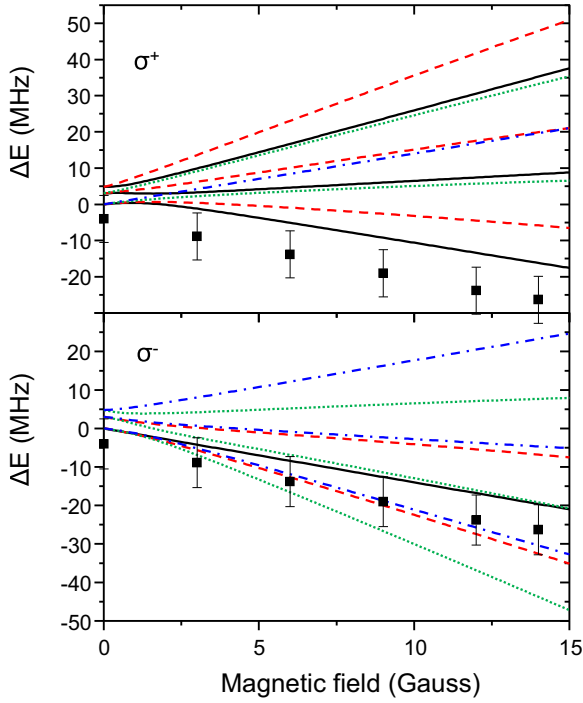
FIG. 6. Energy shift of σ^+ (top) and σ^- transitions (bottom) as a function of the external magnetic field B. Zero energy shift corresponds to $^2S_{1/2}$ $(F = 3/2) \rightarrow$ $^2P_{3/2}$ $(F = 5/2)$ transitions at $B = 0$. The line types represent the magnetic quantum numbers of the ground state. Solid, dashed, dotted, and dash-dotted lines correspond to excitations from the $M_F = -3/2, -1/2, 1/2,$ and $3/2$ ground-state levels, respectively. The data points correspond to the experimental laser frequency at optimum trapping efficiency (see text).
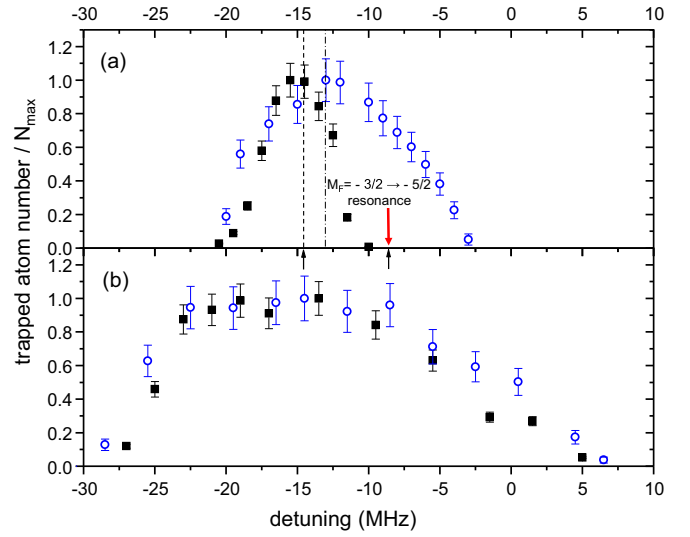

FIG. 7. Relative population in the all-optical trap (solid squares) and standard MOT (open circles) for different laser frequencies. In (a) the data is plotted as a function of the detuning of the cooler beam with respect to the $^2S_{1/2}$ $(F = 3/2) \rightarrow$ $^2P_{3/2}$ $(F = 5/2)$ transition at $B = 0$ for a fixed frequency difference between cooler and repumper beams of 228.5 MHz. The red arrow denotes the resonance frequency of the dominant transition in the σ configuration, i.e., the transition between $M_F = -3/2$ and $-5/2$ for $B = 6$ Gauss. In (b) the data is shown as a function of the repumper frequency shift with respect to the $^2S_{1/2}$ $(F = 1/2) \rightarrow$ $^2P_{3/2}$ $(F = 3/2)$ transition at $B = 0$. The cooler frequency was fixed at a detuning of -14.5 MHz and 13 MHz for the all-optical trap and MOT, respectively.

for both σ^+ and σ^- but not π transitions (i.e., $\Delta M_F = -1$ or $+1$ but not 0). In Fig. 6, the Zeeman shifts of all possible σ^+ (top) and σ^- (bottom) transitions between the ground and excited levels are shown as a function of the magnetic field. The data points in the graph correspond to the incoming laser beam frequency with the error bars accounting for the natural linewidth (5.8 MHz), the estimated Doppler broadening (for 2 mK), and the bandwidth of the laser system ($\sim$1 MHz).

As seen from Fig. 6, there are σ^- transitions close to the experimental cooling laser frequency for all ground-state sublevels, while for the σ^+ transitions the light is significantly farther off resonance except for the $M_F = -3/2$ ground state. Notably, the electric dipole matrix element of the corresponding σ^+ transition ($M_F = -3/2$ to $-1/2$) is at least a factor of 2.4 (depending on the magnetic field strength) smaller than of the σ^- transition from the same ground state. Therefore, σ^+ transitions are generally suppressed resulting in significant optical pumping to the states with the smallest M_F. This conjecture is underpinned by the dependence of the incoming laser frequency on the magnetic field which follows closely the Zeeman shift of the transition $M_F = -3/2 \rightarrow -5/2$ and is consistently about 4–8 MHz red-detuned to this resonance (represented by the solid line in the bottom graph of Fig. 6 and indicated by the arrow in Fig. 5).

Information on the polarization of the target cloud can also be obtained by measuring the polarization of the fluorescence

signal (details are found in Ref. [12]). In the σ configuration, the fluorescence photons are emitted in σ^-, π, and σ^+ transitions with relative contributions of 93%, 5%, and 2% corresponding to a degree of polarization of 90%. This high degree of polarization is consistent with the optical pumping mechanism discussed above resulting in a closed cooling cycle between the $(F, M_F) = (3/2, -3, 2)$ and $(5/2, -5/2)$ states with only a small leak due to σ^+ excitation.

For the π configuration a much lower degree of polarization is observed (see Table II). Here, the cooling beams in x and y directions are linearly polarized with their electric field vectors being parallel to the magnetic field and are driving only π transitions. The beams along the z axis are also linearly polarized and can lead to σ^+ and σ^- transitions with the latter being dominant due to a smaller detuning. Consequently, optical pumping effects are inhibited in this configuration.

The effect of the laser frequencies on trapping properties of the AOT was further investigated and compared to the standard MOT configuration. For the first measurement, the cooler and the repumper frequencies were varied simultaneously but their frequency offset was kept constant at about 228.5 MHz [see Fig. 7(a)]. In the second measurement, the cooler frequency remained constant while the repumper frequency was changed [Fig. 7(b)]. Both traps, AOT and MOT, are relatively insensitive to changes in the repumper frequency and in a region of more than 15 MHz no significant drop in trap population is observed. However, both traps behave differently with respect to alterations of the cooler frequency: While for the MOT the

frequency can still be varied by about 5 MHz without affecting the trap performance, the AOT exhibits a significantly narrower frequency dependence with the optimum at about 6 MHz red-detuned to the resonance energy of the dominant transition.

IV. TRAPPING MECHANISM

In general, there are two types of forces acting on a two-level atom exposed to the field of a monochromatic laser beam: the gradient force (or optical dipole force) oriented along the field intensity gradient, and the scattering force (or spontaneous force) in the direction of the Poynting vector. While these forces are very well understood and tremendous successes have been achieved in the theoretical description of many subtle cooling and trapping mechanisms, the explanation of the properties of laser-cooled samples remains to be an extremely challenging task (e.g., [18]) owing to the complexity of real-world experimental systems, and there are still questions left unanswered. For instance, there is to our knowledge no complete and consistent explanation for the phenomenon of "supermolasses"—first observed by Chu *et al.* [8]—reported in literature. The present configuration has obvious resemblances to the supermolasses and other atom traps with similar laser beam geometries [9–11]. We, too, presently do not have a full model that explains all features of our trapped gas cloud. However, based on our experimental results we can still draw conclusions about the effects that are relevant for the dynamics in the present atom trap.

Compared to earlier traps, the present σ configuration is particularly clean and simple in two respects: First, any spatial dependence of the forces can only be related to variations in the optical field itself because all other fields (in particular the magnetic field) are homogeneous. Second, position and velocity dependent optical pumping effects, that can give rise to spatial confinement (e.g., [19,20]), are minimized. This is because all laser beams drive the same σ^- transitions with respect to a "universal" quantization axis (except for a small contribution of σ^+ transitions). Therefore, the cooling cycle is almost closed between two magnetic substates making it an effective two-level system.

For the present experimental conditions, the force exerted on the atoms by a single monochromatic laser beam is vastly dominated by the spontaneous force which exceeds the optical dipole force by about six orders of magnitude. This suggests that the present configuration could be described by a simplistic optical molasses model including only the spontaneous force exerted on two-level atoms. Although it has been shown that a scattering force alone—if merely proportional to the photon flux—cannot result in a stable trapping of atoms [21] it was earlier claimed that stable trajectories can exist in systems with misaligned laser beams due to a damped vortex motion [9] or due to a dynamical stabilization process similar to the Kapitza pendulum [22]. We performed a three-dimensional Monte Carlo simulation using the optical molasses picture described in Ref. [23], where the experimental geometry was accounted for by implementing six Gaussian laser beams with adjustable powers, widths, and positions. We tested this model by examining two scenarios. First, we simulated the trap loss rate due to the random walk of the atoms. Second, we tried to

reproduce the trap loading by the atom capture out of the cold beam from the 2D-MOT.

In the first simulation, we considered an ideal optical molasses with perfectly aligned laser beams of equal intensity. Here, the trapping time is limited due to the heating caused by the re-emission of photons and it amounts to about 0.5 s. These results are consistent with earlier simulations and experimental observations (e.g., [8]). In our experiment there is a substantial imbalance in laser intensities due to losses at the view ports and the back-reflecting mirrors. For laser beam parameters as listed in Table I the simulation yields a trapping time of about 30 ms which vastly underestimates the experimentally observed trapping time of more than 5 s.

In order to investigate the capture process of atoms out of the loading beam, we first measured the velocity distribution of the incoming atoms with the MOTReMi by photo-ionizing the ^{6}Li atoms from the trap and from the loading beam, respectively, with an ultraviolet laser. By comparing the fragments' momentum distribution, the atom beam velocity was determined to be about 35 ± 10 m/s. We simulated the interaction of the cooling lasers with the atom beam entering the trap region roughly along the bisecting line between the x and the y axes. It is found that none of the atoms are captured in the trap but they are either back-reflected or guided around the trapping volume without resulting in a significant accumulation of atoms in the trap region. Both tests of our Monte Carlo model clearly indicate that the classical optical molasses picture is insufficient to describe the dynamics in the present experiment.

There is a vast amount of literature dealing with alterations of the light forces exerted on atoms due to features not included in our model (e.g., [24]) among them the multilevel structure of the ^{6}Li atoms, the multichromaticity of the incoming light, and spatial interference structures of the six laser beams. In optical lattices, for instance, interference structures between intersecting monochromatic laser beams form periodic and microscopic trapping potentials. While the potential depth of each lattice site would be much too shallow to trap atoms in the present experiment, introducing a second frequency to the laser field drastically changes the situation and results in bichromatic forces (for a recent example see [25]). For our system with one laser frequency very close to the atomic resonance (i.e., the cooler frequency) and the second one shifted off the resonance (the repumper frequency), the bichromaticity results in a rectification of the dipole force, an effect first proposed by Kazantsev and Krasnov [26].

In a simple picture [27], this effect can be understood as follows: Depending on the difference of the two wavelengths and the distance to the retro-reflecting mirror, the fields of the two frequencies will create standing waves that are offset to one another at the trap region. Due to the ac Stark shift the field being off resonance will slightly alter the atomic resonance frequency thereby spatially modulating the effective detuning of the field that is close to resonance. For an appropriate spatial offset between the two standing waves the optical dipole force, which in a monochromatic standing wave averages to zero on a length scale larger than the wavelength, can be "rectified" because it sensitively depends on the effective detuning. The offset of the two waves depends on the distance to the retro-reflecting mirror and, therefore, a superlattice [28,29] can be formed which features potential wells of much larger depth and

geometrical size than a conventional monochromatic optical lattice.

The influence of the rectified dipole force on cold trapped atoms has been demonstrated earlier [28], and it has been considered in a theoretical atom trap [29]. However, the experimental conditions in Ref. [28] and specific considerations in Ref. [29] are quite different from the present scenario mainly regarding the detuning of the off-resonance frequency but also regarding the beam geometries and polarization. However, an order of magnitude estimate on the strength of the rectified dipole force for the present experiment shows that it also can significantly contribute to the balance in the present trap. Using the model proposed by Kazantsev and Krasnov [26] and assuming an atom at rest located in a one-dimensional standing wave of linear polarization containing two frequencies, the maximum rectified dipole force is approximated by

$$F_{\text{RD,max}} = \frac{1}{2} \hbar k \left| \frac{\Omega_0}{\Delta_0} \right|^4 \frac{|\Omega_1|^2}{\Delta_1}, \qquad (6)$$

where Ω_i and Δ_i are the Rabi frequency and detuning associated with the two wavelengths and k is the wave number associated with the wavelength closest to resonance. Under the present experimental conditions the Rabi frequencies are close in magnitude to their respective detunings and for simplicity the ratios will be approximated to unity. This reduction leads to the order of magnitude approximation of rectified force of

$$F_{\text{RD,max}} \sim \tfrac{1}{2} \hbar k |\Omega_1|. \qquad (7)$$

This can be compared directly to the maximum spontaneous force in a field of monochromatic light,

$$F_{\text{scat}} < \tfrac{1}{2} \hbar k \gamma, \qquad (8)$$

where γ is the natural linewidth for the transition.

The conjecture that the present trapping scheme does not solely rely on the spontaneous force but that the rectified dipole force is significant is supported by some of the experimental observations reported in the previous section. First, the atom loss rate Γ does not saturate in the investigated regime but rather decreases monotonically with raising the laser intensities (Fig. 3). This cannot be explained by the spontaneous force alone because it is expected to saturate at the present laser intensities, which are on average about 2.5–7.5 times the saturation intensity I_{sat} (2.54 mW/cm^2 for the lithium D2 transitions) for each individual beam. Second, the trapped atom number depends more sensitively on the cooler frequency than on the repumper frequency (Fig. 7). This is in accordance with our estimate on the strength of the rectified dipole force [cf. Eq. (6)] which depends stronger on variations in Δ_0 (corresponding to the detuning of the cooler beam and about 6 MHz in our experiment) than in Δ_1 (the frequency offset

of the repumper beam with respect to the cooler transition and here about 215–230 MHz).

It should be noted that in spite of the relatively large maximum magnitude of the rectified force, its spatial periodicity of $\pi/\delta k$ (about 65 cm in the present case) leads to a rather "shallow" well, whose size seems to be too large to confine the atom cloud to a small volume of a few millimeters in diameter. However, in the present case the field polarization and intensity distributions result in a mixture of traveling and standing waves, forming a complex three-dimensional field. This makes the implementation of the rectified dipole force in the above classical molasses model extremely challenging. On the basis of the present analysis, we do not make a conclusive statement here and a critical influence of other unwanted but still present effects (e.g., concentric diffraction patterns of the beams due to imperfect beam collimation with spherical lenses) cannot be ruled out.

V. CONCLUSION

In conclusion, we reported on an all-optical near-resonant ^{6}Li atom trap that—in contrast to conventional magneto-optical traps—does not require magnetic field gradients in the trapping region. This feature along with atom temperatures of only a few mK and number densities of about 10^9 cm^{-3} make the present atom trap ideally suited for kinematically complete ion-electron coincidence experiments in COLTRIM spectrometers. The trap uses the same hardware as magneto-optical traps and can be realized with only small modifications of laser beam geometries and polarization. Therefore, it can easily be implemented in other existing MOTRIMS experiments.

Although a complete theoretical model of the observed trapping mechanism is still pending, it is evident that the spontaneous force alone (i.e., the resonant scattering of photons) is not sufficient to describe the observed features. For the present experimental conditions, the rectified dipole force due to the bichromaticity of the laser field is significant and might contribute to the trapping of the atoms. The fact that similar trapping schemes with other species than lithium have previously been realized makes us confident that the present technique can be exploited for the preparation of a large variety of atomic targets for collision experiments. Using other atomic species—in particular effective two-level systems which do not require repumping (e.g., magnesium)—would allow one to alter the frequency and intensity of the off-resonant part of the laser field and study the influence of the bichromatic force in more detail.

[1] J. Ullrich, R. Moshammer, A. Dorn, R. Dörner, L. P. H. Schmidt, and H. Schmidt-Böcking, Rep. Prog. Phys. **66**, 1463 (2003).

[2] R. Dörner, V. Mergel, O. Jagutzki, L. Spielberger, J. Ullrich, R. Moshammer, and H. Schmidt-Böcking, Phys. Rep. **330**, 95 (2000).

[3] B. D. DePaola, R. Morgenstern, and N. Andersen, Adv. Atom., Mol., Opt. Phys. **55**, 139 (2008).

[4] G. Zhu, M. Schuricke, J. Steinmann, J. Albrecht, J. Ullrich, I. Ben-Itzhak, T. J. M. Zouros, J. Colgan, M. S. Pindzola, and A. Dorn, Phys. Rev. Lett. **103**, 103008 (2009).

[5] A. Leredde, X. Fléchard, A. Cassimi, D. Hennecart, and B. Pons, Phys. Rev. Lett. **111**, 133201 (2013).

[6] R. Hubele, A. LaForge, M. Schulz, J. Goullon, X. Wang, B. Najjari, N. Ferreira, M. Grieser, V. L. B. de Jesus, R. Moshammer, K. Schneider, A. B. Voitkiv, and D. Fischer, Phys. Rev. Lett. **110**, 133201 (2013).

[7] D. Fischer, D. Globig, J. Goullon, M. Grieser, R. Hubele, V. L. B. de Jesus, A. Kelkar, A. LaForge, H. Lindenblatt, D. Misra, B. Najjari, K. Schneider, M. Schulz, M. Sell, and X. Wang, Phys. Rev. Lett. **109**, 113202 (2012).

[8] S. Chu, M. G. Prentiss, A. E. Cable, and J. E. Bjorkholm, in *Laser Spectroscopy VIII: Proceedings of the Eighth International Conference, Åre, Sweden, June 22–26, 1987*, edited by W. Persson and S. Svanberg (Springer, Berlin/Heidelberg, 1987), pp. 58–63.

[9] T. Walker, D. Hoffmann, P. Feng, and R. Williamson, Phys. Lett. A **163**, 309 (1992).

[10] T. Walker, P. Feng, D. Hoffmann, and R. S. Williamson, Phys. Rev. Lett. **69**, 2168 (1992).

[11] A. Höpe, D. Haubrich, H. Schadwinkel, F. Strauch, and D. Meschede, Europhys. Lett. **28**, 7 (1994).

[12] R. Hubele, M. Schuricke, J. Goullon, H. Lindenblatt, N. Ferreira, A. Laforge, E. Brühl, V. L. B. de Jesus, D. Globig, A. Kelkar, D. Misra, K. Schneider, M. Schulz, M. Sell, Z. Song, X. Wang, S. Zhang, and D. Fischer, Rev. Sci. Instrum. **86**, 033105 (2015).

[13] K. R. Overstreet, P. Zabawa, J. Tallant, A. Schwettmann, and J. P. Shaffer, Opt. Express **13**, 9672 (2005).

[14] A. Ridinger, S. Chaudhuri, T. Salez, U. Eismann, D. R. Fernandes, K. Magalhaes, D. Wilkowski, C. Salomon, and F. Chevy, Eur. Phys. J. D **65**, 223 (2011).

[15] N. W. M. Ritchie, E. R. I. Abraham, Y. Y. Xiao, C. C. Bradley, R. G. Hulet, and P. S. Julienne, Phys. Rev. A **51**, R890 (1995).

[16] T. G. Tiecke, S. D. Gensemer, A. Ludewig, and J. T. M. Walraven, Phys. Rev. A **80**, 013409 (2009).

[17] M. Gehm, Ph.D thesis, Duke University, 2003.

[18] O. N. Prudnikov, A. V. Taichenachev, and V. I. Yudin, J. Exp. Theor. Phys. **120**, 587 (2015).

[19] D. E. Pritchard, E. L. Raab, V. Bagnato, C. E. Wieman, and R. N. Watts, Phys. Rev. Lett. **57**, 310 (1986).

[20] N. Cooper and T. Freegarde, J. Phys. B **46**, 215003 (2013).

[21] A. Ashkin and J. P. Gordon, Opt. Lett. **8**, 511 (1983).

[22] V. S. Bagnato, N. P. Bigelow, G. I. Surdutovich, and S. C. Zílio, Opt. Lett. **19**, 1568 (1994).

[23] P. D. Lett, W. D. Phillips, S. L. Rolston, C. E. Tanner, R. N. Watts, and C. I. Westbrook, J. Opt. Soc. Am. B **6**, 2084 (1989).

[24] H. Metcalf and P. van der Straten, *Laser Cooling and Trapping* (Springer-Verlag, Berlin/Heidelberg, 1999).

[25] Z. Feng, S. Ebser, L. Ringena, F. Ritterbusch, and M. K. Oberthaler, Phys. Rev. A **96**, 013424 (2017).

[26] A. P. Kazantsev and I. V. Krasnov, J. Opt. Soc. Am. B **6**, 2140 (1989).

[27] R. Grimm, Y. B. Ovchinnikov, A. I. Sidorov, and V. S. Letokhov, Phys. Rev. Lett. **65**, 1415 (1990).

[28] A. Görlitz, T. Kinoshita, T. W. Hänsch, and A. Hemmerich, Phys. Rev. A **64**, 011401 (2001).

[29] G. Wasik and R. Grimm, Opt. Commun. **137**, 406 (1997).